CORROSION SCIENCE AND TECHNOLOGY, Vol.18, No.3(2019), pp.73~77
[Research Paper]
pISSN: 1598-6462 / eISSN: 2288-6524
DOI: https://doi.org/10.14773/cst.2019.18.3.73

Micro-scale Observation of Corrosion of Hot-Dip Aluminized 11% Cr Stainless Steel

Min-Seung Cho, Choong-Nyeon Park, and Chan-Jin Park†

Department of Materials Science and Engineering, Chonnam National University, 77, Yongbongro, Bukgu, Gwangju 61186, South Korea

(Received May 21, 2019; Revised June 12, 2019; Accepted June 12, 2019)

Hot-dip aluminized coating has been widely used to protect steel substrate against corrosion. In this study, the corrosion behavior of hot-dip aluminized type 409L (11% Cr) stainless steel (SS) was investigated using macro- and micro-scale polarization tests. An Al-Fe-Si alloy layer that was formed due to inter-diffusion of alloying elements between Al coating and SS substrate was observed between Al coating and 409L SS substrate. In both macro- and micro-scale polarization tests, the corrosion potential (E_{corr}) of the 409L SS substrate was much nobler than that of the Al coating and alloy layer. E_{corr} of the alloy layer was between that of Al coating and 409L SS substrate. This indicates that the alloy layer can act as a buffer between the more active Al coating and the nobler SS substrate for pit growth in aluminized SS. The presence of the alloy layer appears to be helpful in hindering pitting corrosion of aluminized SS.

Keywords: *Aluminized stainless steel, Alloy layer, Micro-scale polarization, Pitting corrosion*

1. Introduction

Thus far, hot-dip aluminized steels have been used in the cold-end parts of an exhaust system including the muffler. However, bare stainless steels (SSs) or aluminized SSs exhibiting better corrosion resistance have replaced conventional aluminized steels owing to the extension of the warranty period for muffler systems [1-7]. In particular, aluminized SSs are preferred because they exhibit white-colored rust rather than the negatively regarded red rust in the initial stage of corrosion and have better corrosion resistance than expected owing to the galvanic protection effect of the Al coating [6,7].

However, studies on the development of corrosion in aluminized SSs and the protection of materials from corrosion have rarely been conducted. In particular, an alloy interlayer can be formed between the Al coating and SS substrate [8,9], which may affect the corrosion resistance of aluminized SS. Thus, in this study, we tried to investigate the corrosion mechanism in aluminized 11% Cr ferritic SS.

†Corresponding author: parkcj@jnu.ac.kr

2. Experimental

Commercial hot-dip aluminized type 409L SSs with a 32-μm-thick Al coating and bare type 409L SSs (Fe-11.2 Cr-0.55Si-0.2Ti-0.008C) were used for the tests. The surface and cross-sectional microstructure, and the composition of the SSs were observed using a field emission scanning electron microscope (FE-SEM) and an energy dispersive X-ray spectroscope (EDS). In particular, for the observation of the cross-sectional image of the aluminized SS, the specimens were mounted so that the lateral part was exposed to the outside, and then diamond-polished to a surface finish of up to 1 μm. In addition, the Al coating layer was removed for several seconds in a solution composed of 25 mL of deionized (DI) water, 15 mL of nitric acid, 15 mL of hydrofluoric acid (HF), and 45 mL of hydrochloric acid (HCl). Subsequently, the specimens were cleaned with DI water.

To investigate the electrochemical characteristics of the Al coating layer, alloy interlayer, and SS substrate, we conducted potentiodynamic tests on the surface of the aluminized SS, the alloy interlayer exposed after the surface etching, and the type 409L SS, respectively, in 3.5% NaCl solution at 25 °C. The sample of interest was used as a working electrode, Pt mesh was used as a counter electrode, and saturated calomel electrode (SCE) was used as a reference electrode. In addition, the polarization be-

haviors of the micro-area containing the alloy interlayer were investigated in 0.2 M NaCl solution at 25 °C using a capillary-based droplet cell [10], which was specially designed to observe the electrochemical characteristics of the micro-area including the alloy interlayer. A capillary with a diameter of 25 μm was used for the tests.

3. Results and discussion

Fig. 1 shows the surface and cross-sectional images of the hot-dip aluminized SS. The surface of the Al coating was rough, presumably because of the dendritic growth of the coating (Fig. 1a). The cross-sectional image of the aluminized SS clearly exhibits the alloy interlayer between the type 409L SS substrate and Al coating (Fig. 1b). The thickness of the entire coating layer was approximately 32 μm, including that of the interlayer, which was 5 μm. In the energy dispersive X-ray spectroscopy profile, the interlayer was found to be composed of an Al-Fe-Si compound. In particular, Si enrichment was observed in the interface between the Al coating layer and interlayer (Fig. 1c). This phenomenon appears to be due to the preferential formation of the Al-Fe alloy layer and the resultant outward expulsion of Si.

Fig. 2 shows the morphology and composition of the Al-Fe-Si interlayer exposed after etching the surface Al layer for 1–2 s in a solution of 25 mL of H_2O, 15 mL of HNO_3, 15 mL of HF, and 45 mL of HCl. After pickling, the Al coating layer was dissolved with remaining the Al-Fe-Si interlayer [8,9]. Cracks were observed on the surface of the interlayer. These cracks appeared to have formed during the coiling of the aluminized SS sheet owing to the brittle characteristic of the Al-Fe-Si interlayer that formed between the coating layer and SS substrate. Practically, the brittle characteristic of the alloy interlayer is known to help prevent the excessive growth of the interlayer.

The anodic polarization behaviors of the surface of the bare type 409L SS without the Al coating, the surface of the aluminized SS, and the surface of the interlayer

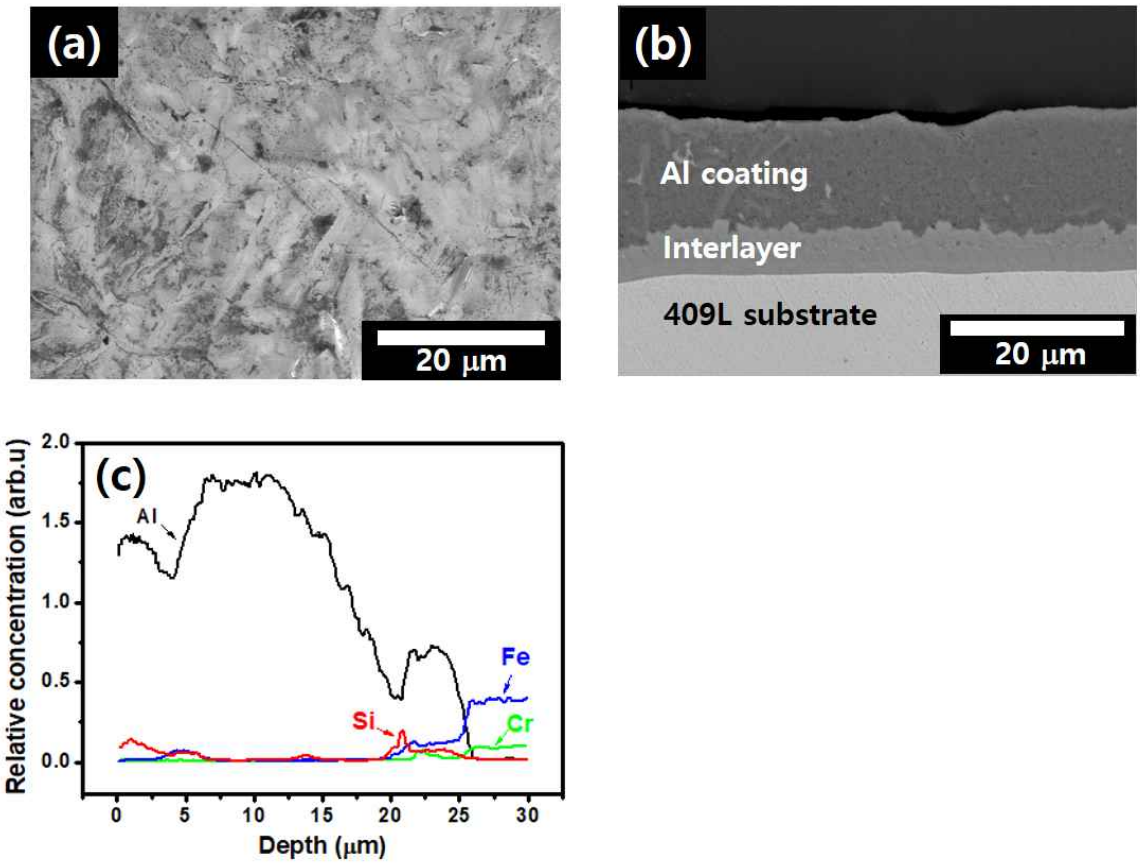

Fig. 1 (a) Surface SEM image, (b) cross-sectional backscattered SEM image, and (c) corresponding compositional energy dispersive X-ray spectroscopy profile of the aluminized stainless steel.

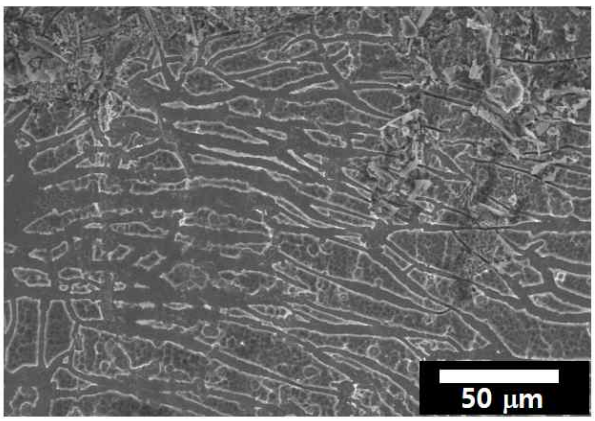

Fig. 2 SEM image of an Al-Fe-Si interlayer exposed after the etching of the surface Al layer.

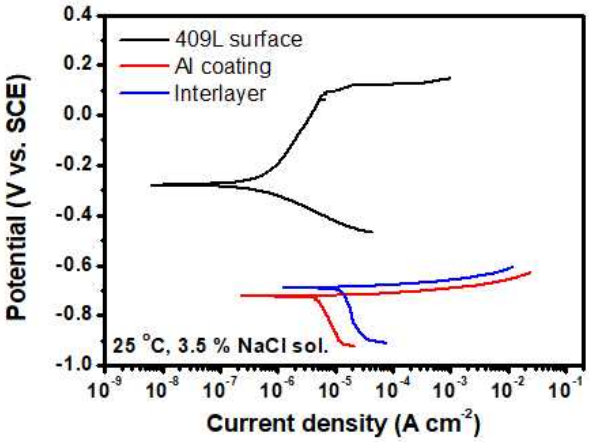

Fig. 3 Potentiodynamic curves of the surfaces of type 409L stainless steel, aluminized 409L stainless steel, and interlayer exposed after the removal of the Al coating.

exposed after removing the Al coating layer were investigated in 3.5% (≈0.6 M) NaCl solution at 25 °C, and the results are shown in Fig. 3. The bare type 409L SS surface, aluminized SS surface, and interlayer surface represent the SS substrate, Al coating layer, and interlayer in an aluminized steel, respectively. The corrosion potential (E_{corr}) of the Al coating (-0.72 V vs. SCE) and interlayer (-0.69 V vs. SCE) was measured to be much lower than that of type 409L SS (-0.28 V vs. SCE). On comparison, E_{corr} of the interlayer was higher than that of the Al coating. A more active E_{corr} of the Al coating and interlayer indicates that these coating layers can successfully act as galvanic protection layers for the type 409L SS substrate. The role of the interlayer is not clear with this result alone. However, it is considered that this layer that formed between the SS substrate and Al coating may act as a buffer layer for rapid pit penetration by mitigating the large E_{corr} difference between the SS substrate and

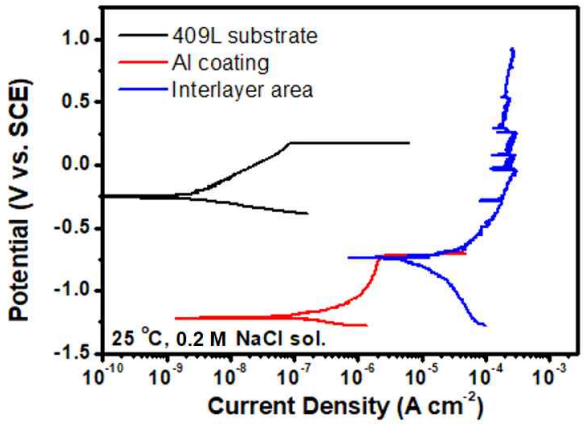

Fig. 4 Potentiodynamic curves of the 409L stainless steel substrate, the Al coating surface, and the micro-area including the interlayer obtained using a capillary-based droplet cell.

Al coating.

The aluminized 409L SSs were mounted with epoxy so that the side of the samples were exposed to the environment and polished, as shown in Fig. 1b. Then, polarization curves were obtained from the 409L SS substrate area and the area including the interlayer. Furthermore, a polarization test was conducted on the Al coating using a capillary-based droplet cell for comparison. Due to the limitation of capillary size, the area including the interlayer part was used for the test. Fig. 4 shows the polarization curves for the type 409L SS substrate, Al coating surface, and micro-area including the interlayer, measured in 0.2 M of NaCl solution at 25 °C. To avoid crevice corrosion in the capillary tip, we slightly decreased the NaCl concentration compared to that used in the macro-polarization test. E_{corr} of the 409L SS surface, Al coating surface, and area including the interlayer was measured to be -0.25, -1.21, and -0.7 V vs. SCE, respectively. In addition, the measured pitting potential (E_{pit}) for the 409L SS and Al coating surface was 0.17 and -0.72 V vs. SCE, respectively. The Al coating showed a passivity behavior different from that observed in the macro-polarization test. This phenomenon may be attributed to the slightly lower chloride concentration and to the lower probability of defects in the micro-area sample. The pitting corrosion was highly dependent on the surface defects in the sample. Generally, a smaller sample area contains fewer total defects that can influence the pitting corrosion. E_{corr} was higher in the order of 409L SS > alloy layer > Al coating. It has been well known that an Al coating layer is more active than a SS substrate and, thus, can act as a sacrificial anode for the substrate. In addition, from this work, it was found that the alloy layer can act

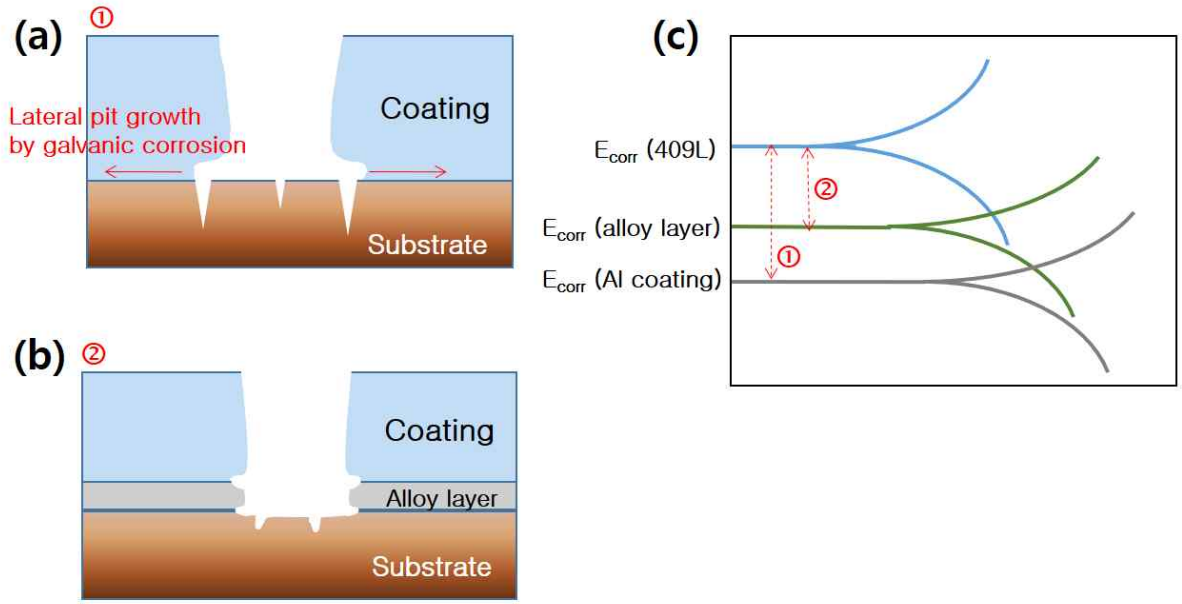

Fig. 5 Schematic of the growth of the pitting corrosion: (a) Al coating on a 409L stainless steel substrate without an alloy layer, (b) Al coating on a 409L stainless steel substrate with an alloy layer, and (c) polarization curves of the 409L stainless steel, alloy layer, and Al coating.

as a buffer layer between the Al coating and 409L SS substrate, and also as an anode for the SS substrate.

The mechanism for pit penetration in aluminized SS is suggested as shown in Fig. 5. In the case of direct Al coating on 409L SS without the alloy layer, the galvanic corrosion effect can be more severe owing to the larger gap in E_{corr} between the Al coating and 409L SS substrate. The propagation of the pit through the Al coating is arrested when the pit reaches the SS substrate. Instead, the pit can grow laterally owing to the large galvanic effect between the Al coating and 409L substrate. However, a highly occluded environment can increase the acidity of the pit and, accordingly, the pit can initiate and grow into the SS substrate further. In contrast, for the case in which the alloy layer is located between the Al coating and SS substrate, the alloy layer can act as a buffer for the pit growth and the severity of the pitting corrosion can be less since E_{corr} of the alloy layer is between that of the Al coating and SS substrate. Accordingly, pitting corrosion can be retarded compared with the case without the alloy layer. Unfortunately, this hypothesis could not be verified perfectly owing to the difficulty in the direct observation of pit growth. Hence, further study is required.

4. Conclusions

The corrosion behavior of aluminized type 409L (11% Cr) stainless steel (SS) was investigated using macro- and micro-scale polarization tests. An Al-Fe-Si alloy layer was observed between the Al coating and 409L SS. In the alloy layer; Si enrichment was observed in the interface between the Al coating and alloy layer owing to the preferential formation of the Al-Fe alloy layer and the resultant outward expulsion of Si. In both, the macro- and micro-scale polarization tests, the corrosion potential (E_{corr}) of the 409L SS substrate was much nobler than that of the Al coating and the alloy layer. E_{corr} of the alloy layer was between that of the Al coating and 409L SS substrate. This indicates that the alloy layer can act as a buffer between a more active Al coating and a nobler SS substrate for the pit growth in the aluminized SS. The presence of the alloy layer appears to be helpful in hindering the pitting corrosion of aluminized SS.

Acknowledgments

This work was supported by POSCO and the National Research Foundation (NRF) of Korea (No. 2016R1A2B4015883).

References

1. M. D. Salgado, S. C. S. Rodrigues, D. M. Santos, A. S. Brandim, and V. F. C. Lins, *Eng. Fail. Anal.*, **79**, 89 (2017).
2. M. -J. Kim, S. -I. Jang, S. -H. Woo, J. -G. Kim, and Y. -H. Kim, *Corrosion*, **71**, 285 (2015).
3. P. H. Han, Z. H. Xu, C. P. Wang, M. C. Li, and H. Y.

Bi, *Int. J. Electrochem. Sci.*, **9**, 3784 (2014).
4. H. P. Kim and D. J. Kim, *Corros. Sci. Tech.*, **17**, 183 (2018).
5. W. -J. Beom, K. -S. Yun, C. -J Park, H. -J. Ryu, and Y. -H Kim, *Corros. Sci.*, **52**, 734 (2010).
6. M. -J Kim, S. -H Woo, and J. -G Kim, *Mater. Trans.*, **56**, 1599 (2015).
7. M. R. Bateni, P. Wei, O. Kesler, and A. Petric, *Mater. Manuf. Process.*, **28**, 1314 (2013).
8. Y. X. Li, Q. Jia, Z. T. Zhu, W. Gao, and H. Chen, *Surf. Rev. Lett.*, **24**, 1750046 (2017).
9. H. T. Zhang and J. K. Liu, *Mat. Sci. Eng. A*, **528**, 19 (2011).
10. Y. -I. Choi, D. Paik, and C. -J. Park, *ECS Electrochem. Lett.*, **1**, C5 (2012).